Supplementary Materials for

Iontronic Array with a Frequency-Coding Architecture for Transient Tactile Perception

Zhibin Li[1] †, Jing Yang[1] † , Yuxuan Zhang[1], Peiyan Geng[1], Jiansong Feng[1], Bin Chen[1], Xu Zhang[1], Guojiang Yuan[1], Xiaolong Chen[1], Taihong Wang[1, 2] *

[1]Department of Electronic and Electrical Engineering,
Southern University of Science and Technology, Shenzhen, Guangdong 518055, P. R.
[2] School of Microelectronics,
Southern University of Science and Technology, Shenzhen, Guangdong 518055, P. R.

*Corresponding author. Email: wangth@sustech.edu.cn
†These authors contributed equally to this work.

This PDF file includes:

- Note S1. Theoretical analysis of AC-based capacitance-to-voltage convertor.
- Note S2. Theoretical analysis of digital quadrature demodulator.
- Note S3. Theoretical analysis of circuit anti crosstalk.
- Note S4. Description of standard capacitance measurement experiment.
- Fig. S1. Structure diagram of digital quadrature demodulator.
- Fig. S2. Analysis of capacitance crosstalk suppression.
- Fig. S3. The experimental circuit for measuring the standard capacitance.
- Fig. S4. Schematic of the preparation of the flexible electrode arrays with microstructures.
- Fig. S5. Signal superposition test circuit.
- Fig. S6. AIM-skin array sensors synchronous response under multi touch.
- Fig. S7. Dynamic response of sensor nodes under single finger sliding.
- Fig. S8. The pressure values of ten dynamic touch gestures with respect to the capture frames and the set of sensor units.
- Fig. S9. Multi channels sinusoidal signal generation circuit based on AD9833.
- Fig. S10. Signal acquisition hardware system diagram. Digital Circuit Design Block Diagram Based on FPGA.
- Fig. S11. Digital Circuit Design Block Diagram Based on FPGA.
- Fig. S12. Res3D architecture.
- Fig. S13. 2D and 3D convolution architecture.
- Fig. S14. Comparison of recognition results of Res3D, C2D and C3D.
- Fig. S15. The classification accuracy of dynamic touch gestures for each participant based on Res3D.
- Tables S1. Touch Gestures with Description.
- Tables S2. The Confusion Matrix for Result Evaluation.

Other Supplementary Materials for this manuscript include the following:

Movies S1 to S3

Supplementary Notes

Note S1. Theoretical analysis of AC-based capacitance-to-voltage convertor.

The output voltage of the C/V convertor can be expressed as:

$$V_o'(t) = \sum_{i=0}^{7} -\frac{R_f}{j\omega_i C_f R_f + 1} \cdot j\omega_i C_i \cdot V_i(t) \qquad (1-1)$$

where $V_o'(t)$ is the output signal of the C/V converter on the row interface number o, and o = 0, 1, ..., 7, ω_i is the angular frequency of the excitation source. C_i is the capacitance on the different column addresses being measured, which can be expressed by solving the corresponding frequency path voltage amplitude:

$$C_i = \left| -\frac{j\omega_i C_f R_f + 1}{j\omega_0 V_i(t) R_f} \right| \cdot V_o^i(t) = \frac{\sqrt{\left(\omega_i C_f R_f\right)^2 + 1}}{\omega_i R_f} \cdot \frac{A_o^i}{A_i} \qquad (1-2)$$

where A_i is the amplitude of the input AC excitation voltage signal $V_i(t)$ with angular frequency ω_i, and A_o^i is the amplitude of the output AC signal $V_o^i(t)$ with angular frequency ω_i. Therefore, the solution of A_o^i requires the following digital quadrature demodulation. To analyze the dynamic performance of the C/V converter, we solve its response under the action of a single frequency ω_0, and the transfer function is expressed as:

$$V_o'(t) = -\frac{R_f}{j\omega_0 C_f R_f + 1} \cdot j\omega_0 C_0 \cdot V_0(t) \qquad (1-3)$$

$$G(s) = \frac{V_o'(s)}{V_0(s)} = -\frac{R_f}{sC_f R_f + 1} \cdot sC_0 = \frac{sC_0}{C_f}\left(-\frac{C_f R_f}{sC_f R_f + 1}\right) \qquad (1-4)$$

which is a first-order system, with a time constant τ being $C_f R_f$. Assuming that $\frac{C_0}{C_f} = K$, Eq. (4) can be rewritten as:

$$G(s) = K\left(-\frac{s\tau}{s\tau + 1}\right) = \frac{K}{s\tau + 1} - K \qquad (1-5)$$

When a unity step voltage is applied to the C/V converter, the output becomes:

$$V_o'(s) = \frac{1}{s} G(s) = \frac{1}{s}\left(\frac{K}{s\tau + 1} - K\right) \qquad (1-6)$$

By inverse Laplace transform, the output $V_o'(t)$ in the time domain can be expressed as:

$$V_o'(t) = -Ke^{-\frac{t}{\tau}} \qquad (1-7)$$

The response time of the system is defined as the time elapsed for the system to reach a steady state error less than a given value after applying a unit step voltage. When the steady-state error is less than 0.1%, the response time can be calculated as:

$$t_{cv} \geq 6.9\tau \qquad (1-8)$$

For the AIM-skin system, the capacitance of our sensor unit is between 10^{-12}~10^{-9}F. Therefore, according to Eq. (1-3), we need to select the appropriate C_f, R_f so that the output voltage $V_o'(t)$ would be within the appropriate range of ADC. However, according to Eq. (1-8), when $C_f R_f$ is too large, the response time would be too long to affect the normal measurement. Therefore, we need to weigh the C_f, R_f settings. Here, our excitation frequency is 10 kHz to 17 kHz, and we set the response time to be 10% of one signal cycle. Therefore, according to Eq. (1-8), the response security time can be expressed as

$$\tau \leq \frac{t_{cv}}{6.9} \leq \frac{1}{6.9} \cdot \frac{1}{10 f_{17kHz}} \leq \frac{1}{1173\,000} \qquad (1-9)$$

In order to ensure that C/V converter output is acceptable within the measurement range and has high sensitivity, it should be high. The sensitivity is:

$$S_{cv} = \frac{V_o'(t)}{C_0} \qquad (1-10)$$

By introducing Eq. (1-3) the sensitivity can be expressed as:

$$S_{cv} = \left| -\frac{j\omega_0 V_0(t) R_f}{j\omega_0 C_f R_f + 1} \right| = \frac{\omega_0 R_f A_0}{\sqrt{\left(\omega_0 C_f R_f\right)^2 + 1}} \qquad (1-11)$$

where A_0 is the modulus value of $V_0(t)$. We use ADC7606, whose voltage input range is 5 V_{P-P}. Assuming that the maximum capacitance to be measured is 10 nF, the sensitivity of the C/V converter should be 0.0005 V_{P-P}/pF. When the excitation frequency is 17 kHz and the excitation voltage amplitude is 0.2 V_{P-P}, Eq. (1-11) can be expressed as:

$$\frac{0.0005}{10^{-12}}\ \mathrm{V}_{P-P}/\mathrm{F} = \frac{2\pi \cdot 17\,000 \cdot R_f \cdot 0.2}{\sqrt{\left(2\pi \cdot 17\,000 C_f R_f\right)^2 + 1}} \mathrm{V}_{P-P}/\mathrm{F} \qquad (1-12)$$

By combining Eq. (1-9) and Eq. (1-12), the feedback resistance and capacitance can be determined to be:

$$\begin{gathered} R_f \leq 23.50\mathrm{k}\Omega, \\ C_f \geq 36.27\mathrm{pF}. \end{gathered} \qquad (1-13)$$

Therefore, when we set the feedback resistance and capacitance to 20kΩ and 40pF respectively, let the C/V converter's sensitivity and response time meet 0.0005 V_{P-P}/pF and 10% of a signal cycle as much as possible.

Note S2. Theoretical analysis of digital quadrature demodulator.

From Eq. (1-2), we need to solve the amplitude of the mixed frequency output signal to characterize the node capacitance of the corresponding frequency coding. According to Eq. (1-1), the output signal is composed of M sine components (M is 8 in our design). Assume that there are M signals of different frequency sinusoidal components and their superimposed outputs are as follows:

$$y(t) = \sum_{m=1}^{M} A_m \cos(\omega_m t + \varphi_m) + \varepsilon(t) \tag{2 − 1}$$

where A_m, ω_m and φ_m are the amplitude, angular frequency and phase of the m-th sinusoidal component of the signal y, and ε is the measurement noise associated with y. The data after discrete digital sampling by ADC with sampling frequency of f_s is：

$$y(n) = \sum_{m=1}^{M} A_m \cos\left(\omega_m \frac{n}{f_s} + \varphi_m\right) + \varepsilon(n), n = 1,2, \ldots \tag{2 − 2}$$

where n is the serial number of the sample, ω_m is the angular frequency of the m-th sinusoidal component. Eq. (2-2) is represented by matrix as follows:

$$y(n) = \boldsymbol{u}_n \cdot \boldsymbol{x} + \varepsilon(n) \tag{2 − 3}$$

Where $\boldsymbol{u}_n$ is the sine component of the known target frequency, $\boldsymbol{x}$ is the state vector composed of amplitude and phase. $\boldsymbol{u}_n$ and $\boldsymbol{x}$ are expressed as:

$$\boldsymbol{u}_n = \begin{bmatrix} \cos\left(\omega_1 \frac{n}{f_s}\right) \\ \cos\left(\omega_2 \frac{n}{f_s}\right) \\ \vdots \\ \cos\left(\omega_M \frac{n}{f_s}\right) \\ \sin\left(\omega_M \frac{n}{f_s}\right) \\ \vdots \\ \sin\left(\omega_2 \frac{n}{f_s}\right) \\ \sin\left(\omega_1 \frac{n}{f_s}\right) \end{bmatrix}^T, \boldsymbol{x} = \begin{bmatrix} A_1 \cos(\varphi_1) \\ A_2 \cos(\varphi_2) \\ \vdots \\ A_M \cos(\varphi_M) \\ -A_M \sin(\varphi_M) \\ \vdots \\ -A_2 \sin(\varphi_2) \\ -A_1 \sin(\varphi_1) \end{bmatrix} \tag{2 − 4}$$

where the operator $[\ ]^T$ denotes the transpose. When ADC samples N discrete data points, Eq. (2-3) can be expressed as:

$$\boldsymbol{Y}_N = \boldsymbol{U}_N \cdot \boldsymbol{x} + \varepsilon_N \tag{2 − 5}$$

where $\boldsymbol{Y}_N$ is a sample vector of length N, $\boldsymbol{U}_N$ is a sample matrix consisting of $2M$ sine cosine orthogonal components with different frequencies, and the discrete length is N, ε is the error vector. The specific composition is as follows:

$$\begin{aligned} \boldsymbol{Y}_N &= [y(1) \quad y(2) \quad \dots \quad y(N)]^T, \\ \boldsymbol{U}_N &= [\boldsymbol{u}_1 \quad \boldsymbol{u}_2 \quad \dots \quad \boldsymbol{u}_N]^T, \\ \boldsymbol{\varepsilon}_N &= [\varepsilon(1) \quad \varepsilon(2) \quad \dots \quad \varepsilon(N)]^T, \end{aligned} \tag{2-6}$$

From Eq. (1-2), we need to solve the amplitude of the mixed frequency output signal to characterize the node capacitance of the corresponding frequency coding. The amplitude and phase can be represented by the state matrix $\boldsymbol{x}$.

$$\begin{cases} A = \begin{bmatrix} A_1 \\ A_2 \\ \vdots \\ A_M \end{bmatrix} = \begin{bmatrix} \sqrt{\boldsymbol{x}(1)^2 + \boldsymbol{x}(2M)^2} \\ \sqrt{\boldsymbol{x}(2)^2 + \boldsymbol{x}(2M-1)^2} \\ \vdots \\ \sqrt{\boldsymbol{x}(M)^2 + \boldsymbol{x}(M+1)^2} \end{bmatrix}, \\ \varphi = \begin{bmatrix} \varphi_1 \\ \varphi_2 \\ \vdots \\ \varphi_M \end{bmatrix} = \begin{bmatrix} \arccos\left[\frac{x(1)}{A_1}\right] \\ \arccos\left[\frac{x(2)}{A_2}\right] \\ \vdots \\ \arccos\left[\frac{x(M)}{A_M}\right] \end{bmatrix} \end{cases} \tag{2-7}$$

where $\boldsymbol{x}(i)$ is the i-th element of $\boldsymbol{x}$. Therefore, $\boldsymbol{x}$ is the goal of our matrix solution. According to Eq. (2-5), our solution is as follows:

$$\boldsymbol{x} = \boldsymbol{U}_N^{-1} \cdot (\boldsymbol{Y}_N - \varepsilon_N) \tag{2-8}$$

The least squares method can be used to obtain an estimate of $\boldsymbol{x}$:

$$\boldsymbol{x} = (\boldsymbol{U}_N^T \boldsymbol{U}_N)^{-1} \boldsymbol{U}_N^T (\boldsymbol{Y}_N - \boldsymbol{\varepsilon}_N) \tag{2-9}$$

Take Eq. (2-6) into Eq. (2-9) and simplify it as follows:

$$\boldsymbol{x} = \begin{bmatrix} \sum_{n=1}^{N} \cos^2\left(\omega_1 \frac{n}{f_s}\right) & \sum_{n=1}^{N} \cos\left(\omega_1 \frac{n}{f_s}\right)\cos\left(\omega_2 \frac{n}{f_s}\right) & \cdots & \sum_{n=1}^{N} \cos\left(\omega_1 \frac{n}{f_s}\right)\sin\left(\omega_1 \frac{n}{f_s}\right) \\ \sum_{n=1}^{N} \cos\left(\omega_2 \frac{n}{f_s}\right)\cos\left(\omega_1 \frac{n}{f_s}\right) & \sum_{n=1}^{N} \cos^2\left(\omega_2 \frac{n}{f_s}\right) & \cdots & \sum_{n=1}^{N} \cos\left(\omega_2 \frac{n}{f_s}\right)\sin\left(\omega_1 \frac{n}{f_s}\right) \\ \vdots & \vdots & \vdots & \vdots \\ \sum_{n=1}^{N} \sin\left(\omega_1 \frac{n}{f_s}\right)\cos\left(\omega_1 \frac{n}{f_s}\right) & \sum_{n=1}^{N} \sin\left(\omega_1 \frac{n}{f_s}\right)\cos\left(\omega_2 \frac{n}{f_s}\right) & \cdots & \sum_{n=1}^{N} \sin^2\left(\omega_1 \frac{n}{f_s}\right) \end{bmatrix}^{-\mathbf{1}} \cdot \left[\sum_{n=1}^{N} \cos\left(\omega_1 \frac{n}{f_s}\right) y(n) \quad \dots \quad \sum_{n=1}^{N} \cos\left(\omega_M \frac{n}{f_s}\right) y(n) \sum_{n=1}^{N} \sin\left(\omega_M \frac{n}{f_s}\right) y(n) \dots \sum_{n=1}^{N} \sin\left(\omega_1 \frac{n}{f_s}\right) y(n)\right]^T \tag{2-10}$$

In order to simplify the solution of the above $\boldsymbol{x}$, we need to make the above integral length N meet the integer period of each sinusoidal component in the multi frequency signal, so that the unnecessary sinusoidal part can be removed：

$$\begin{cases} \sum_{n=1}^{N} \cos\left(\omega_\alpha \frac{n}{f_s}\right)\cos\left(\omega_\beta \frac{n}{f_s}\right) = \begin{cases} \frac{N}{2} (\alpha = \beta \ and \ \alpha, \beta = 1,2 \dots M) \\ 0 (\alpha \neq \beta \ and \ \alpha, \beta = 1,2 \dots M) \end{cases} \\ \sum_{n=1}^{N} \sin\left(\omega_\alpha \frac{n}{f_s}\right)\sin\left(\omega_\beta \frac{n}{f_s}\right) = \begin{cases} \frac{N}{2} (\alpha = \beta \ and \ \alpha, \beta = 1,2 \dots M) \\ 0 (\alpha \neq \beta \ and \ \alpha, \beta = 1,2 \dots M) \end{cases} \\ \sum_{n=1}^{N} \cos\left(\omega_\alpha \frac{n}{f_s}\right)\sin\left(\omega_\beta \frac{n}{f_s}\right) = 0 \ (\alpha, \beta = 1,2 \dots M) \end{cases} \tag{2-11}$$

When Eq. (2-11) is satisfied, it can be obtained according to Eq. (2-10):

$$x = \frac{2}{N}\left[\sum_{n=1}^{N}\cos\left(\omega_1\frac{n}{f_s}\right)\ldots\sum_{n=1}^{N}\cos\left(\omega_M\frac{n}{f_s}\right),\sum_{n=1}^{N}\sin\left(\omega_M\frac{n}{f_s}\right)\ldots\sum_{n=1}^{N}\sin\left(\omega_1\frac{n}{f_s}\right)\right]y(n)(2-12)$$

The above N length accumulation process is equivalent to a low-pass filter to reduce the measurement noise and retain the DC component. Then calculate the amplitude and phase of the sine component of the signal according to Eq. (2-7) and Eq. (2-12):

$$\begin{cases} A_M = \sqrt{\boldsymbol{x}(M)^2 + \boldsymbol{x}(M+1)^2} \\ \varphi_M = \arccos\left[\dfrac{x(M)}{A_M}\right] \end{cases} \qquad (2-13)$$

$$\begin{cases} A_m = \sqrt{\boldsymbol{x}(m)^2 + \boldsymbol{x}(2M+1-m)^2} \\ \varphi_m = \arccos\left[\dfrac{x(m)}{A_m}\right] \end{cases} \quad (m = 1,2\ldots M) \qquad (2-14)$$

Similarly, we can decompose it into the expression of quadrature demodulation according to Eq. (2-12):

$$\begin{cases} I_m = \dfrac{1}{N}\displaystyle\sum_{n=1}^{N}\cos\left(\omega_m\frac{n}{f_s}\right)\cdot y(n) = \frac{1}{N}\sum_{n=1}^{N}\frac{A_m}{2}\left(\cos\left(2\omega_m\frac{n}{f_s}+\varphi_m\right)+\cos(\varphi_m)\right) \\ Q_m = \dfrac{1}{N}\displaystyle\sum_{n=1}^{N}\sin\left(\omega_m\frac{n}{f_s}\right)\cdot y(n) = \frac{1}{N}\sum_{n=1}^{N}\frac{A_m}{2}\left(\sin\left(2\omega_m\frac{n}{f_s}+\varphi_m\right)+\sin(-\varphi_m)\right) \end{cases}$$

$$(2-15)$$

When the length N of the sampled data meets the integer period of the target frequency or the data sequence is low-pass filtered, the result is:

$$
\begin{cases} I_m &= \frac{1}{2} A_m \cos(\varphi_m) \\ Q_m &= -\frac{1}{2} A_m \sin(\varphi_m) \end{cases} \quad (2-16)
$$

Therefore, the results of amplitude and phase through digital quadrature demodulation are shown as follows:

$$
\begin{cases} A_m = 2 \cdot \sqrt{{I_m}^2 + {Q_m}^2} \\ \varphi_m = \arccos\left[\frac{I_m}{Q_m}\right] \end{cases} \quad (m = 1,2 \dots M) \quad (2-17)
$$

The structure of a single quadrature demodulator is shown in **Fig. S1**. We can solve I_m and Q_m of the target frequency signal through reference signals of different frequencies.

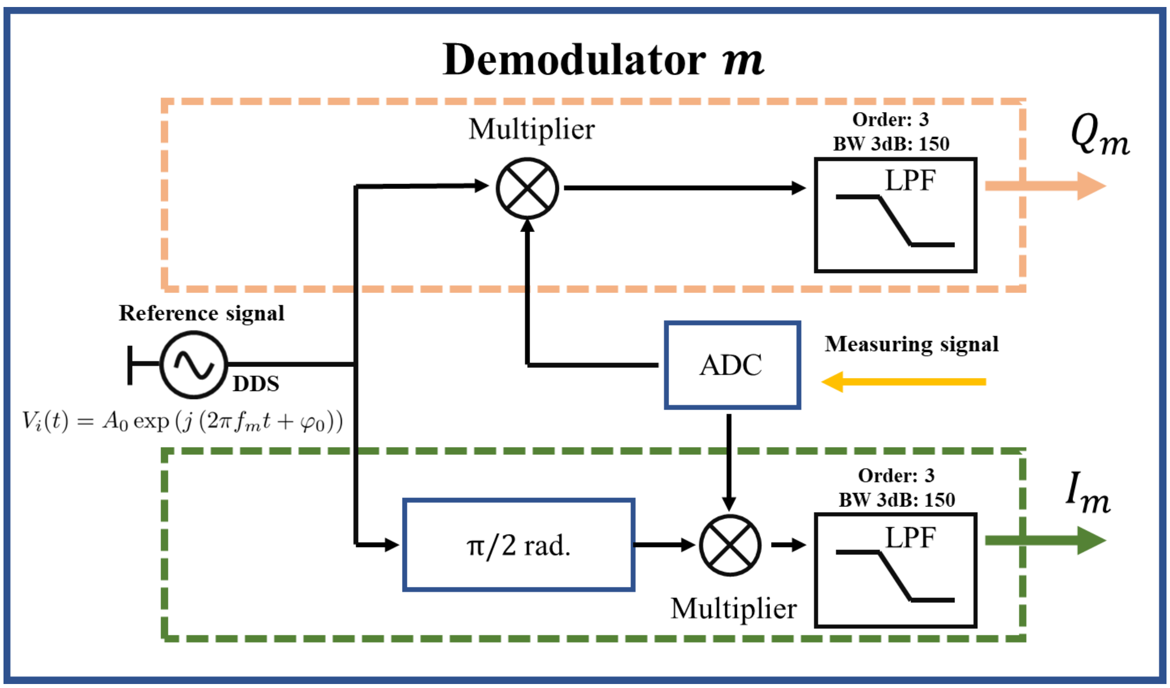

Fig. S1. Structure diagram of digital quadrature demodulator.

Note S3. Theoretical analysis of circuit anti crosstalk.

In our measurement circuit, our crosstalk avoidance is based on the operational amplifier in the C/V converter. In the actual circuit, we hope that when measuring capacitance C_1, it would not be affected by crosstalk caused by parallel connection of other capacitors. We take capacitor C_1 as an example to prove that it is not affected by the change of parallel capacitance in the circuit. As shown in **Fig. S2 A**, this is the array circuit structure diagram and capacitor C_1 local crosstalk equivalent circuit diagram. Under the action of excitation voltage signal V_0 and capacitor C_1 to be measured, the current I_1 passing through capacitor C_1 is:

$$I_1 = V_0 \cdot jwC_1 \qquad (3-1)$$

Where w is the angular frequency of the AC excitation voltage. Under the effect of parallel capacitor, the current finally entering C/V conversion can be expressed as:

$$I_1'' = I_1 + I_1' \qquad (3-2)$$

As shown in **Fig. S2 A**, I_1' is the current passing through other crosstalk capacitors of parallel circuits. However, due to the virtual short characteristic of the operational amplifier, the two-point potentials of U_1 and U_2 are equal to GND. Therefore, the current I_1' can be solved as:

$$I_1' = \frac{U_2 - U_1}{\frac{1}{jwC_9} + \frac{1}{jwC_{10}}} = 0 \qquad (3-3)$$

According to Eq. (3-2) and Eq. (3-3), $I_1'' = I_1$ can be obtained, so the current injected into the operational amplifier is completely through the current of the target capacitor, which is not subject to the crosstalk of parallel capacitors. The result shows that our circuit can effectively suppress the crosstalk caused by the change of parallel capacitance.

In the circuit simulation of Simulink, we set C_1 to 20pf, change the value of all other capacitors in the array, and test the influence of C_1 measurement value. As shown in **Fig. S2 B**, we set all other capacitors on the array to 1pF, 20pF, 50pF, 100pF, 500pF, and 1000pF, respectively. The error between the measured value and the actual value of C_1 is less than 6%.

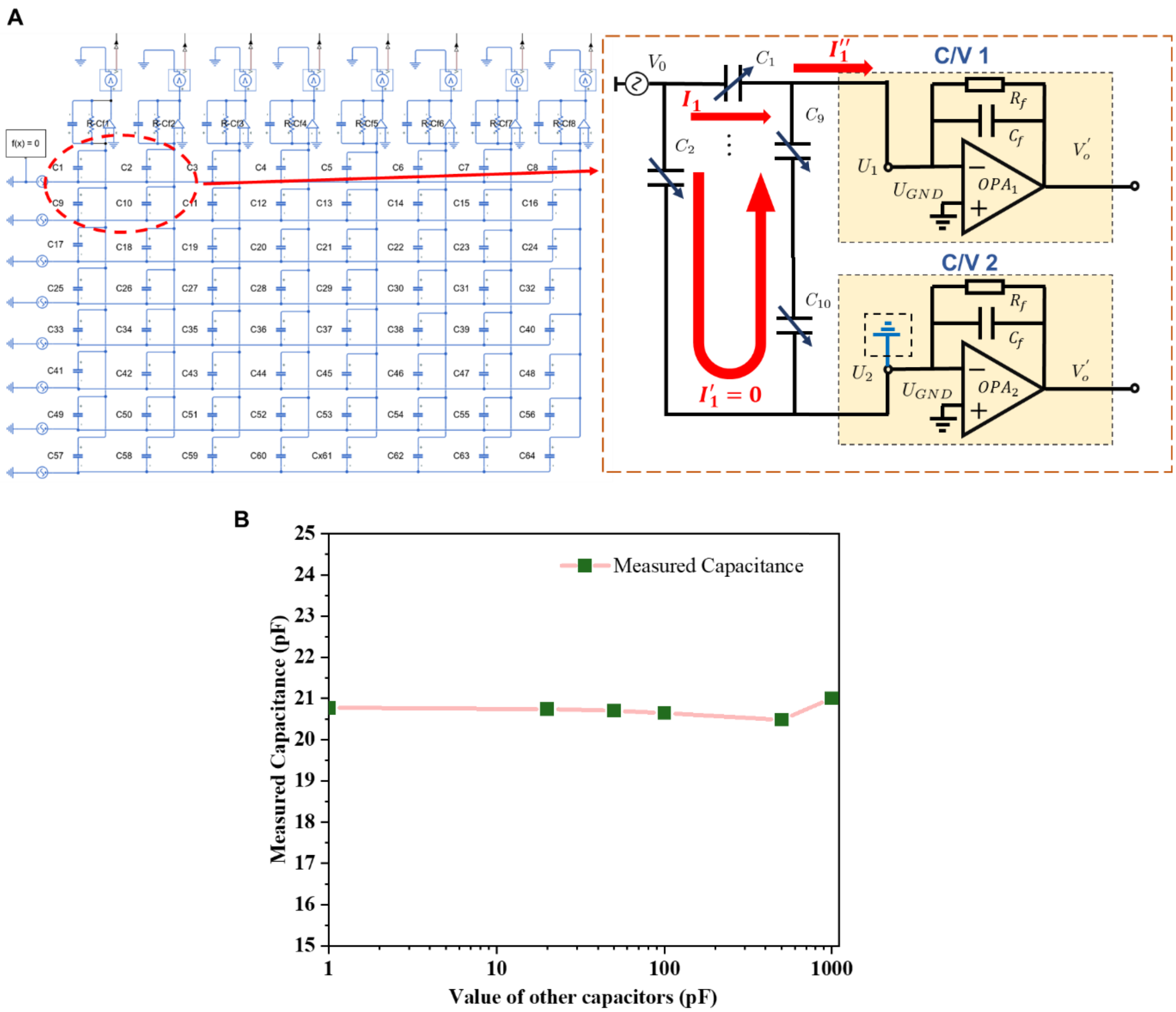

Fig. S2. Analysis of capacitance crosstalk suppression. (A) Array circuit structure diagram and local capacitance crosstalk equivalent circuit diagram. (B) The response diagram of measuring capacitance value when changing other capacitance values on the array in Simulink's circuit simulation.

Note S4. Description of standard capacitance measurement experiment.

We use a single C/V converter verified in **Note S1** to measure the target capacitance, and then use a digital quadrature demodulator to demodulate the signal on the corresponding frequency code. The experimental circuit for measuring the standard capacitance is shown in **Fig. S3**. The experimental circuit for measuring the standard capacitance is shown in Figure 3. We place the capacitance to be measured at the node excited by a 13kHz signal, and the capacitance of other nodes is initialized to 30pF. The amplitude of excitation voltage and noise voltage is 200mV. We set standard capacitors C_x of different values to verify the capacitance measurement accuracy.

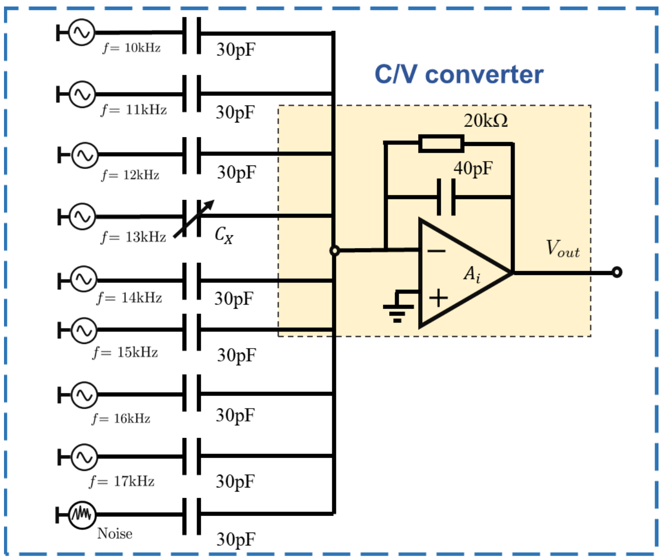

Fig. S3. The experimental circuit for measuring the standard capacitance.

According to Eq. (1-3), we can calculate the capacitance to be measured as follows:

$$C_x = \frac{\sqrt{\left(\omega_i C_f R_f\right)^2 + 1}}{\omega_i R_f} \cdot \frac{A_m}{A_i} \qquad (4-1)$$

where $A_i = 200$ mv is the amplitude of the input AC excitation voltage signal with angular frequency $\omega_i = 2\pi f_i$, and A_m is the amplitude of the output AC signal with angular frequency ω_i. Wherein, A_m can be demodulated and solved according to Eq. (2-17).

Supplementary Figures

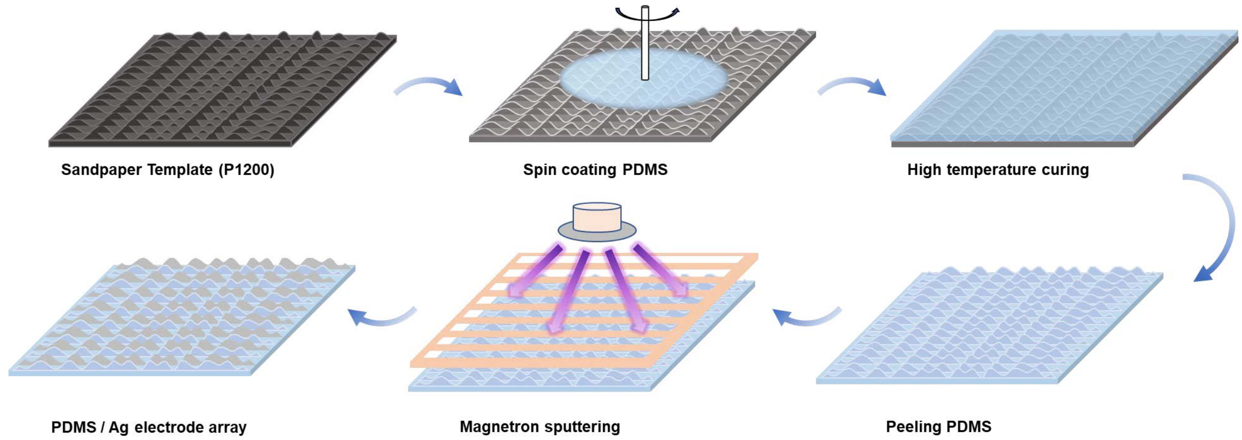

Fig. S4. Schematic of the preparation of the flexible electrode arrays with microstructures. The sandpaper of P1200 is chosen as the template for the microstructure. Flexible PDMS substrate with abundant microstructures is prepared by the template method. By magnetron sputtering, a 200 nm Ag-patterned electrode arrays on PDMS is obtained.

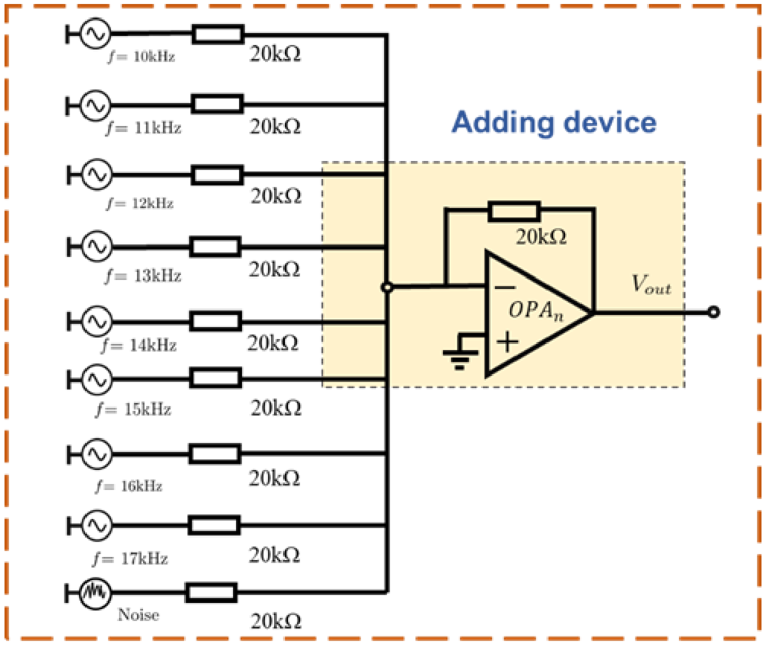

Fig. S5. Signal superposition test circuit. We superimpose the Sine waves with the frequency of 10 kHz, 11 kHz and ...17 kHz, with the amplitude set to 20 mV, and add the noise signal with the amplitude of 20 mV. The output of the superimposed analog signal is used to evaluate the demodulation performance of the demodulator.

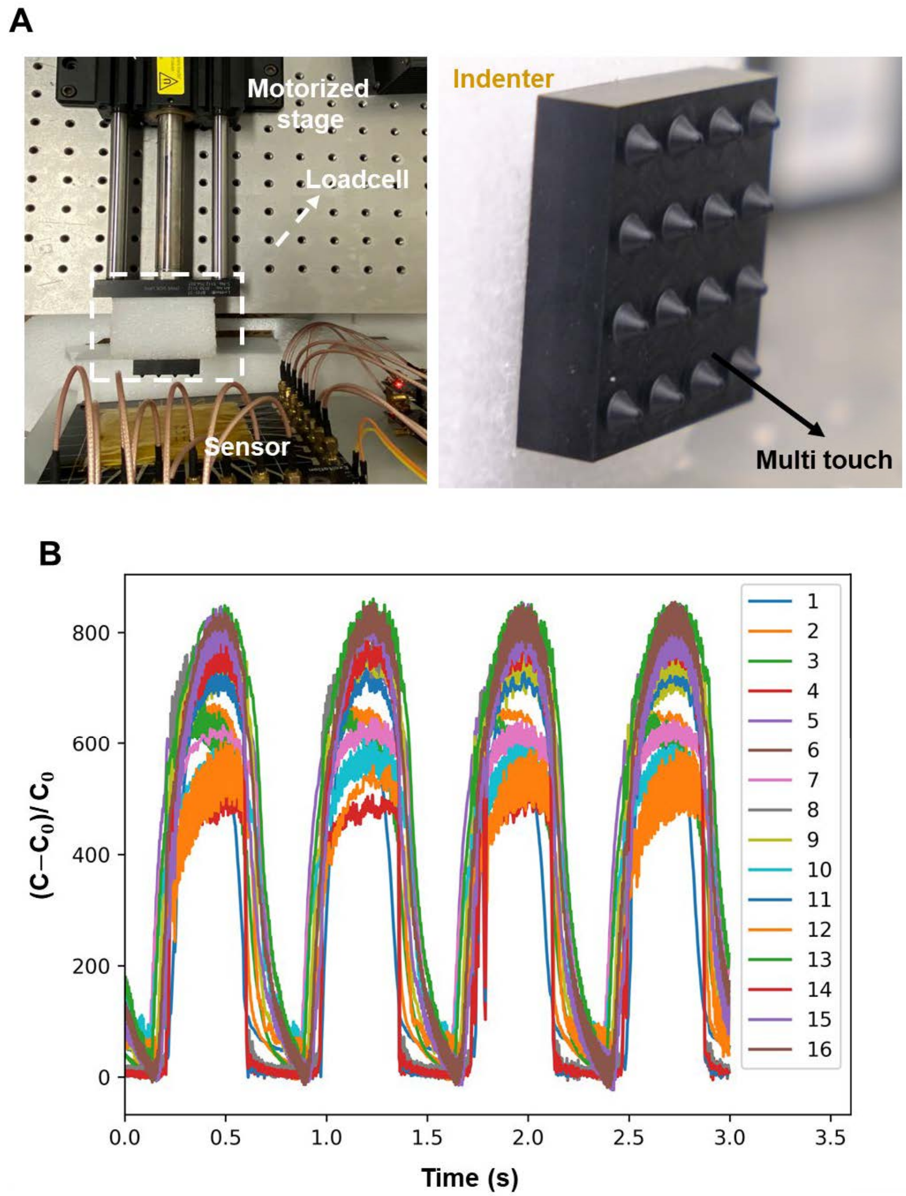

Fig. S6. AIM-skin array sensors synchronous response under multi touch. (A) Experimental platform for multi-touch sensing using AIM-skin array. (B) The capacitance response of 16 contacts under reciprocating touch of linear motor. Sensor nodes can achieve rapid synchronous response.

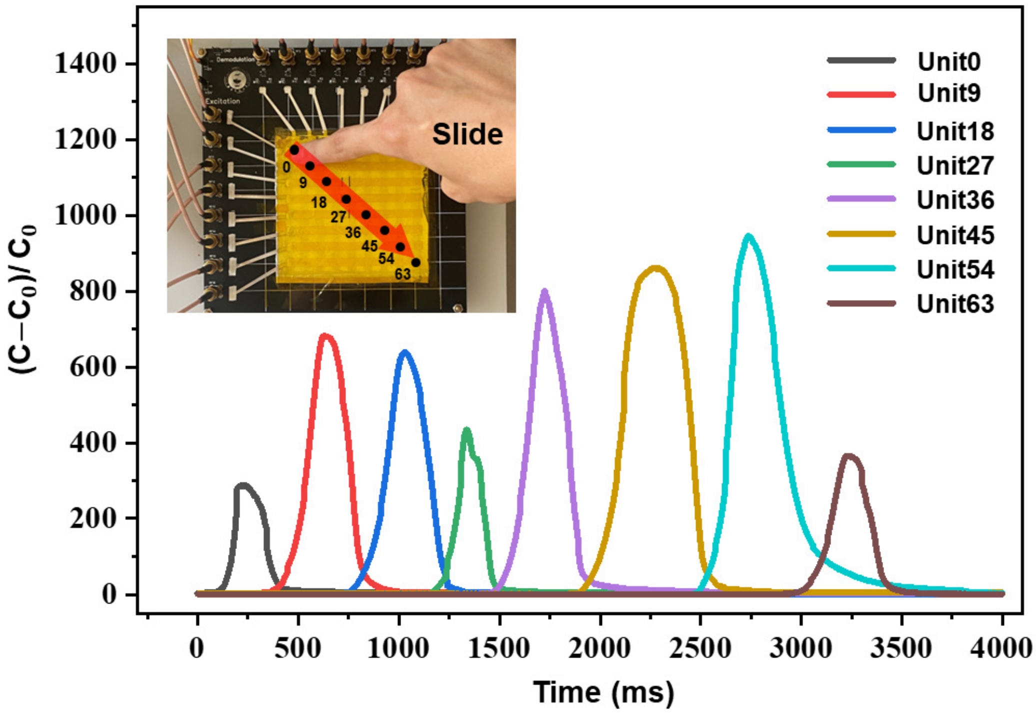

Fig. S7. Dynamic response of sensor nodes under single finger sliding.

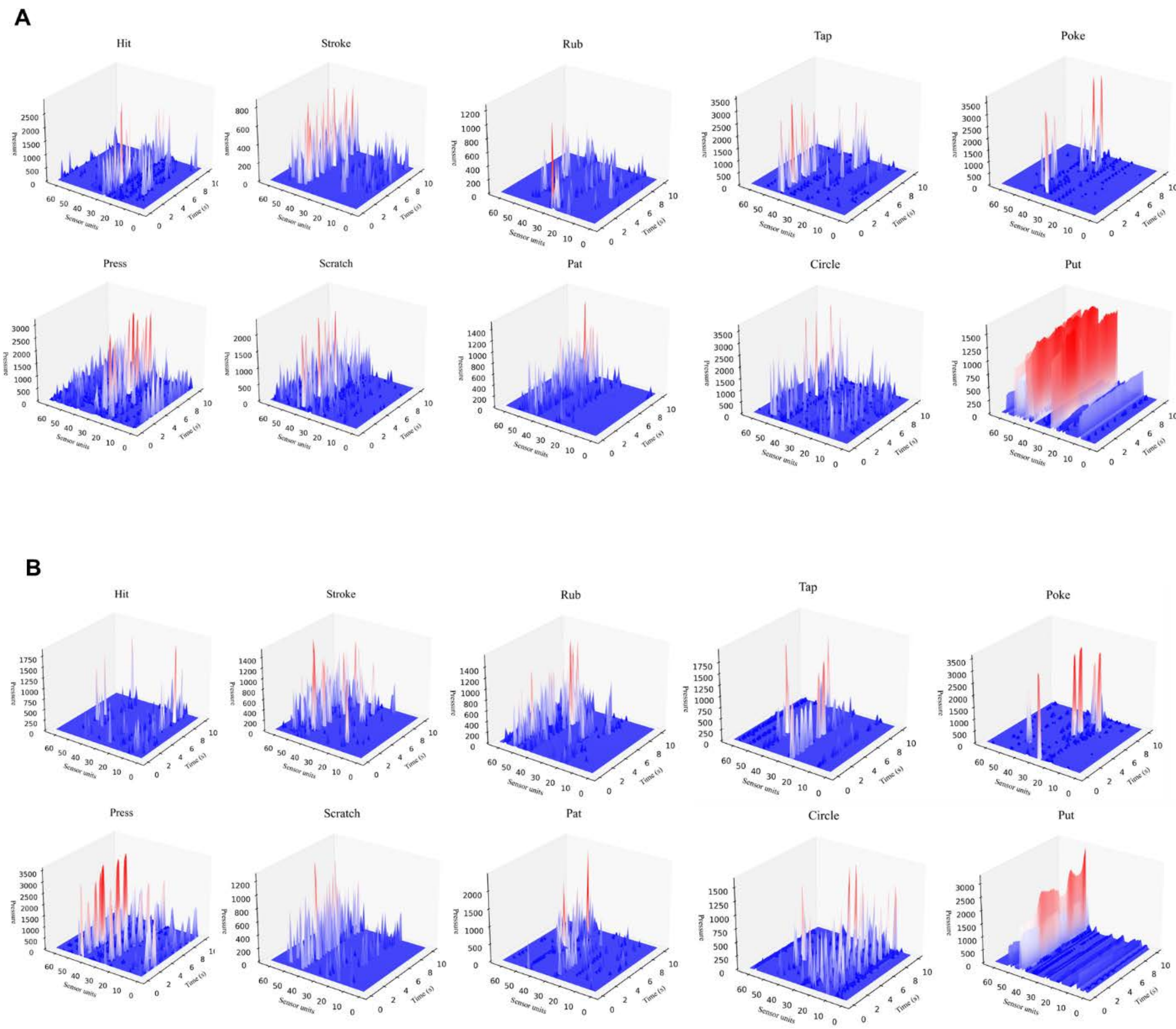

Fig. S8. The pressure values of ten dynamic touch gestures with respect to the capture frames and the set of sensor units. The pressure response (z-axis) with respect to capture time frames (x-axis) and the set of the sensor units (y-axis) for ten dynamic touch gestures that were collected from 2 subjects. Among them, (A) is the No. 1 experiment participant, (B) is the No. 15 experiment participant.

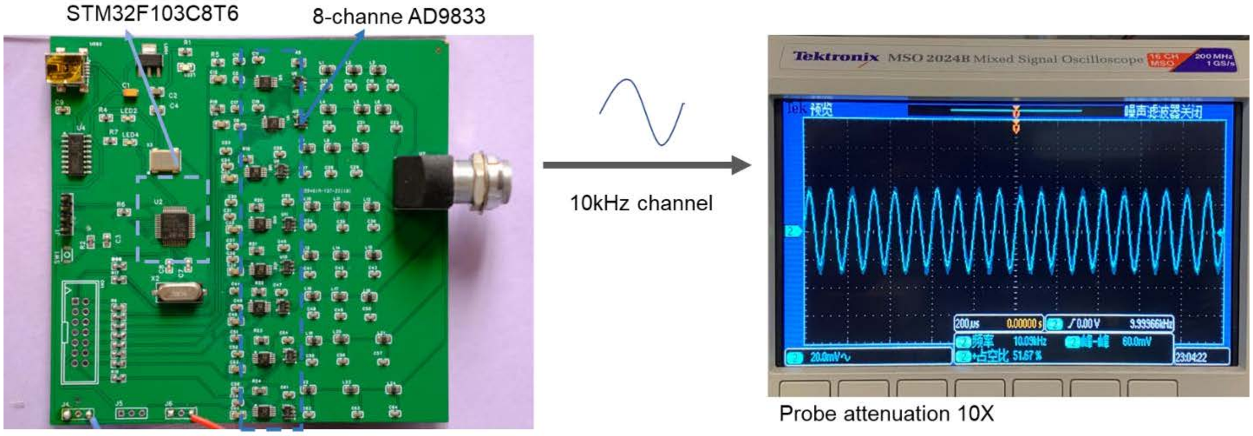

Fig. S9. Multi channels sinusoidal signal generation circuit based on AD9833. We generate sinusoidal signals with frequencies of 10kHz, 11kHz and... 17kHz, and use them as excitation sources for different frequency coding.

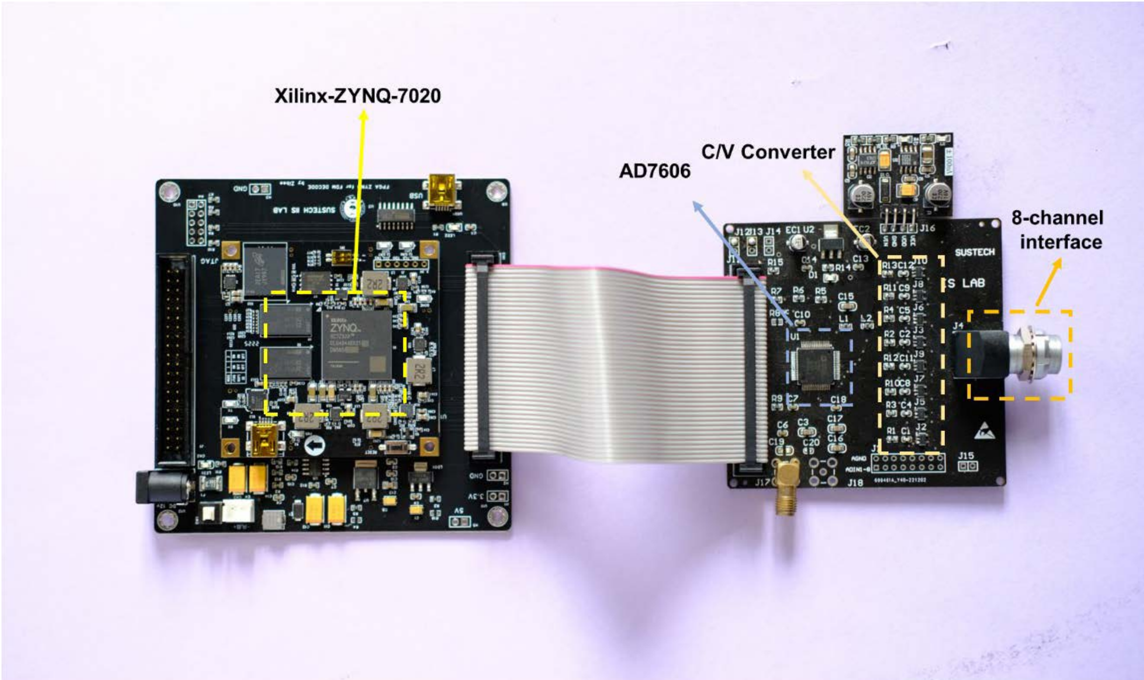

Fig. S10 Signal acquisition hardware system diagram. AD7606 collects the voltage signal after C/V conversion, and FPGA demodulates the digital signal in parallel.

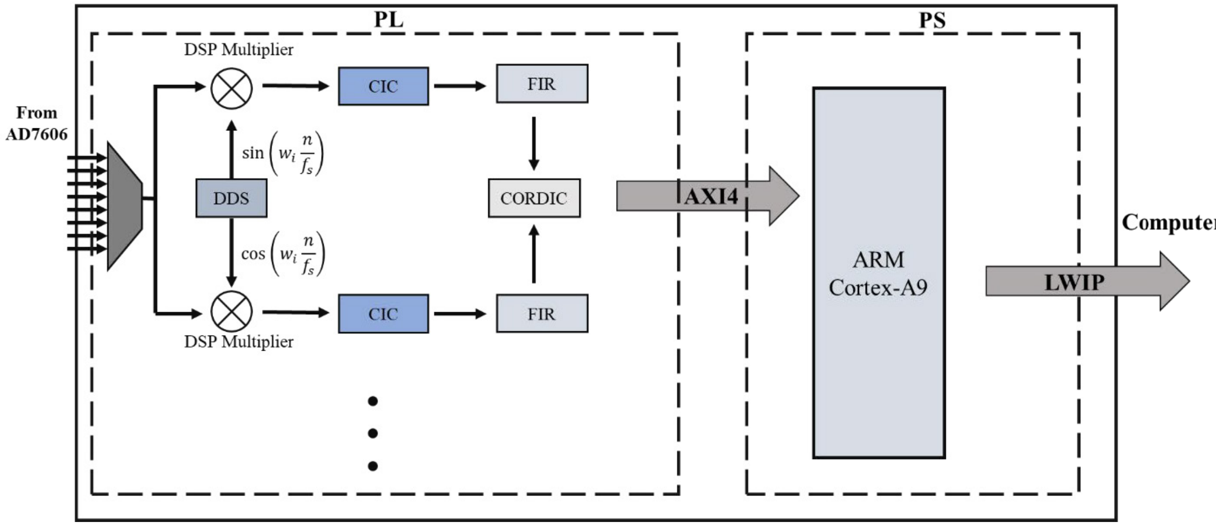

Fig. S11. Digital Circuit Design Block Diagram Based on FPGA. The internal DDS generates two frequency orthogonal reference signals, the DSP multiplies the input signal and the reference signal, and the Cascaded Integrator-Comb (CIC) filter and Finite Impulse Response (FIR) filter realize the low-pass filtering of the signal to obtain the DC component. CORDIC module calculates the root mean square of two signals. The final solution value is transmitted to the PS side through AXI4 link, and ARM packages the data stream and sends it to the upper computer. The CIC filter is used as a decimator for downsampling, with an input sampling rate of 200 kbps and a decimation factor of 40. The FIR filter has a sampling rate of 5 kbps, a cutoff frequency of 150 Hz, and the order of 10.

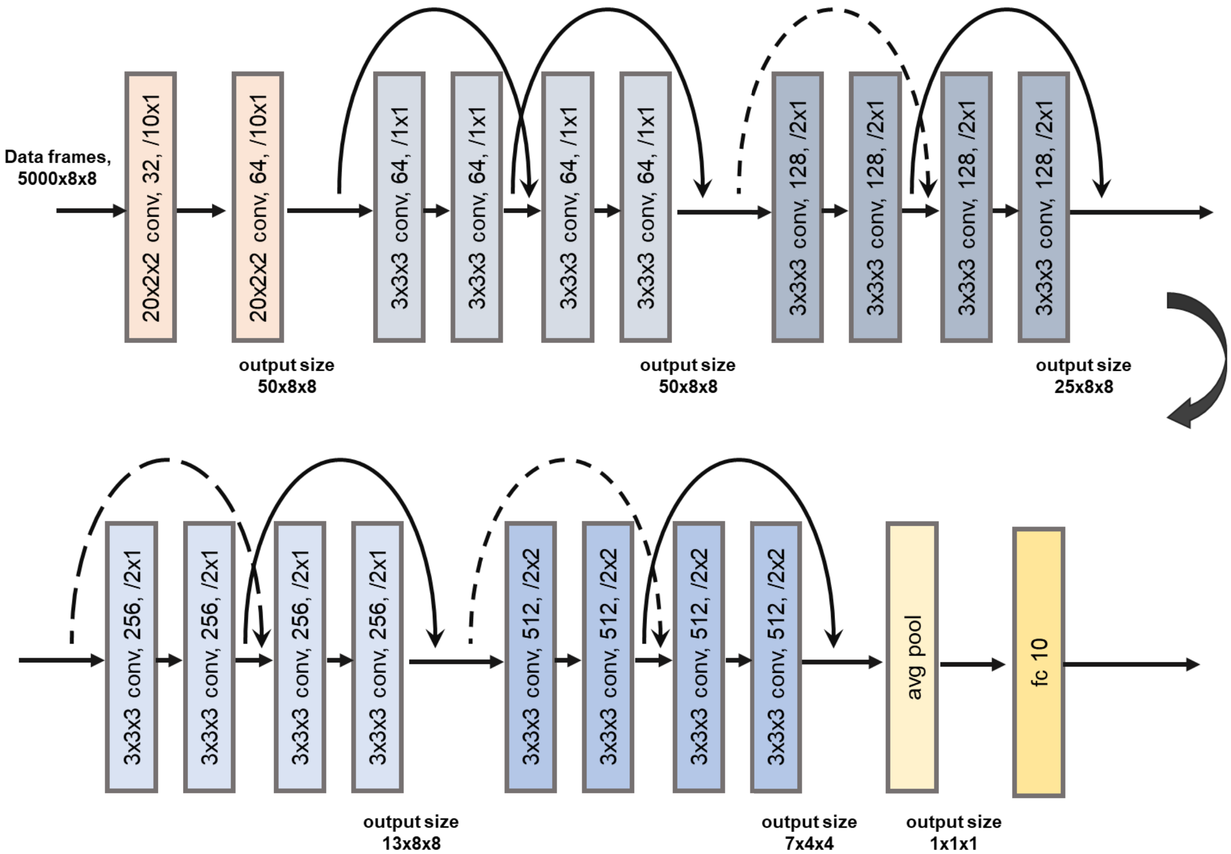

Fig. S12. Res3D architecture. Downsampling strides are denoted as $\boldsymbol{t} \times \boldsymbol{s}$ where $\boldsymbol{t}$ and $\boldsymbol{s}$ are temporal and spatial stride, respectively. Dotted lines are residual connections with downsampling.

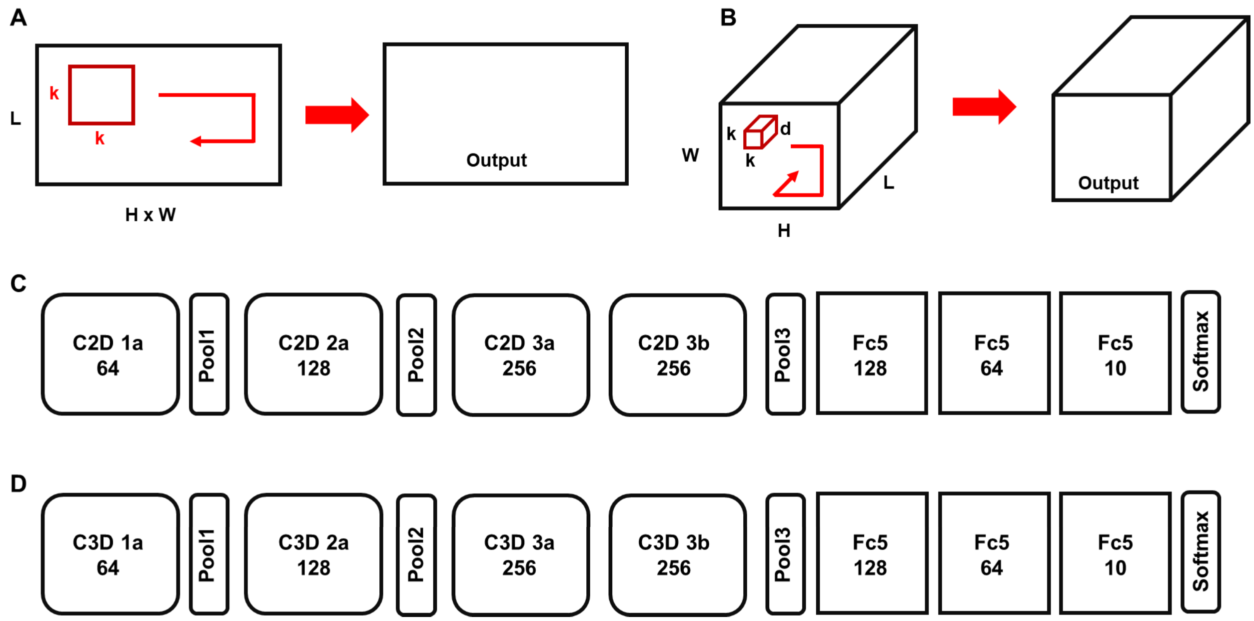

Fig. S13. 2D and 3D convolution architecture. (A) Applying 2D convolution on a touch data volume (multiple frames flattened as one plane) also results in an image. (B) Applying 3D convolution on a touch data volume results in another volume, preserving spatiotemporal information of the input signal. (C) C2D net has 4 2D convolution, 3 max-pooling, and 3 fully connected layers, followed by a softmax output layer. (D) C3D net has 4 3D convolution, 3 max-pooling, and 3 fully connected layers, followed by a softmax output layer.

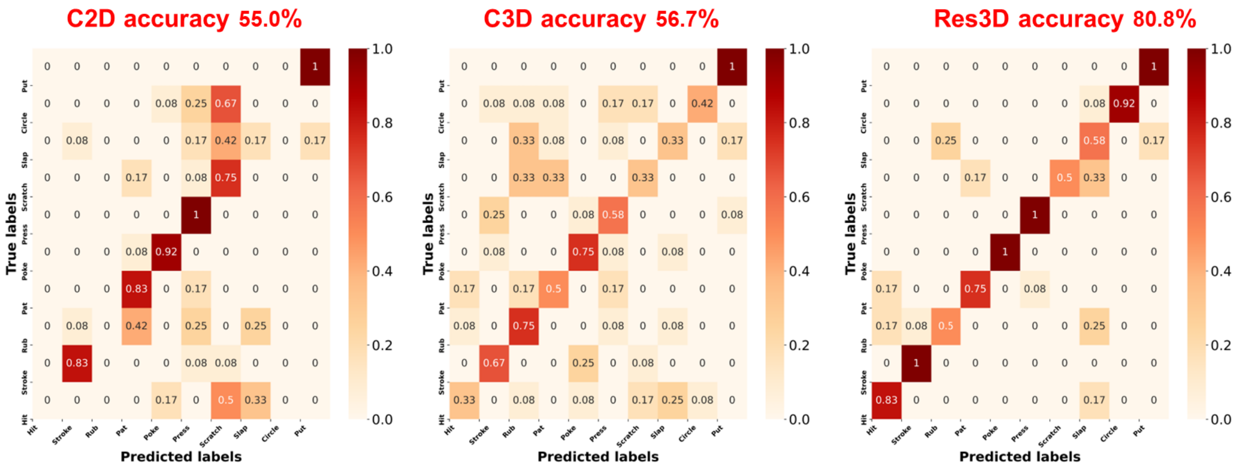

Fig. S14. Comparison of recognition results of Res3D, C2D and C3D. Res3D has significantly improved the recognition accuracy compared with C2D and C3D, which would effectively assist the dynamic gesture recognition of the dynamic tactile sensing system.

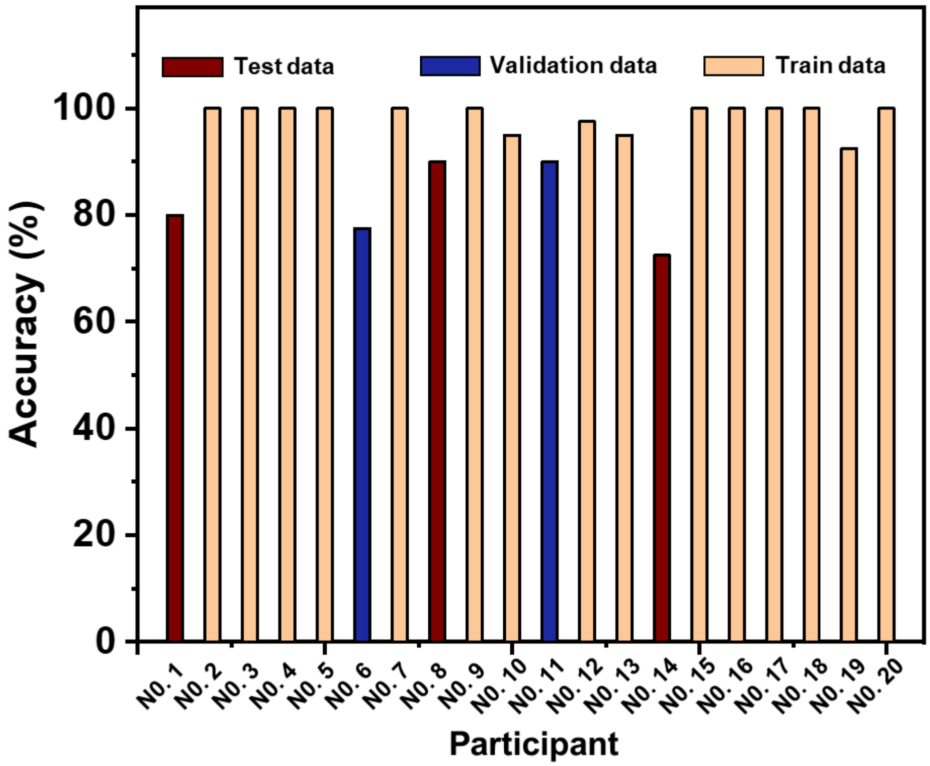

Fig. S15. The classification accuracy of dynamic touch gestures for each participant based on Res3D.

TABLE S1. Touch Gestures with Description

number	gesture	description
A	Hit	Give a blow to the robot with a closed fist quickly and forcefully
B	Stroke	Move your hand gently and slowly over the robot along the same direction
C	Rub	Move your hand backwards and forwards over the robot while pressing firmly
D	Tap	Hit the robot quickly and lightly with your fingers
E	Poke	Push the robot quickly with one finger
F	Press	Push the robot closely and firmly with a steady force
G	Scratch	Rub the robot with your fingernails
H	Pat	Touch the robot gently with your hand flat
I	Circle	Draw a circle on the robot with one finger
J	Put	Place your hand gently on the robot and stay still

Table S1. Touch Gestures with Description. The experimenter completes the above touch actions in turn at the system prompt.

TABLE S2. The Confusion Matrix for Result Evaluation

Predict / Label	True	False
True	*TN*	*FP*
False	*FN*	*TP*

Table S2. The Confusion Matrix for Result Evaluation.

Movie S1.
Capacitive Response of AIM-skin Array.

Movie S2.
Visualization of Spatial Response of the FC-AIMS Platform.

Movie S3.
Construction of AIM-skin tactile perception model.